Contents

1 Introduction

2 Investigated system

2.1 Circuit

2.2 Model in continuous time

2.3 Model in discrete time

$$\theta_{n+1} = F(\theta_n) \bmod 2\pi \tag{1}$$

2.4 Bifurcation structure

3 Archetypal model

3.1 Idea of the approach

The original model is suitable for numerical investigation of the systems dynamics. However, it has a major drawback common for many similar models defined by implicit equations. In fact, this model can be seen as a kind black box, providing no information on how the system dynamics may change under parameter variation.
Since exactly this question is pivotal for the bifurcation analysis, we propose the following approach for investigation of the bifurcation structure exhibited by the original model:

- First, we identify the characteristic properties of the original model at the parameter values leading to the considered bifurcation structure.
- Then, construct a simple model possessing these properties
- Next, we investigate the constructed models and provide an explanation of the considered bifurcation structure.
- Eventually, we validate to which extent the predictions made based on the simplified model apply to the original one.

3.2 Properties of the original map

Proceeding according to the approach described above, let us first identify the properties the map (1) which we assume to be relevant for the formation of the bifurcation structure the map exhibits in the considered parameter domain. As illustrated in Fig. **??**:

- The function F governing the dynamics of map (1) is discontinuous and consists, in the phase interval $[2, 2\pi)$, of four continuous branches denoted in the following by $F_{\mathcal{A}}$, $F_{\mathcal{B}}$, $F_{\mathcal{C}}$ and $F_{\mathcal{D}}$. The domains in the state space associated with these branches are referred to as $I_{\mathcal{A}}$, $I_{\mathcal{B}}$, $I_{\mathcal{C}}$ and $I_{\mathcal{D}}$, respectively, with $I_{\mathcal{A}} \cup I_{\mathcal{B}} \cup I_{\mathcal{C}} \cup I_{\mathcal{D}} = [2, 2\pi)$. The appearance of discontinuities of F is explained by the effect described in [**?**] and related to the tendencies of the flow of the underlying model in continuous time to a boundary of the hysteresis zone. In the following, the discontinuities separating the $I_{\mathcal{A}}$, $I_{\mathcal{B}}$, $I_{\mathcal{C}}$ and $I_{\mathcal{D}}$ from each other a denoted by d_0, d_1, d_2, d_3, where d_0 is the boundary between $I_{\mathcal{D}}$ and $I_{\mathcal{A}}$, d_1 is the boundary between $I_{\mathcal{A}}$ and $I_{\mathcal{B}}$, and so on.
- The function F fulfills the symmetry

$$F(x + \pi) = F(x) + \pi \tag{2}$$

  Therefore, the shapes of the branches $F_{\mathcal{A}}$, $F_{\mathcal{C}}$, as well as $F_{\mathcal{B}}$, $F_{\mathcal{D}}$ are identical, and the distance between the discontinuities d_0, d_2, as well as between d_1, d_3 is equal π.
- Branches of F are non-monotonous. Note that the appearance of local minima and maxima of F is described in [**?**] and – similar to the points of discontinuities – is related to tangencies of the flow in the underlying continuous time model and a boundary of the hysteresis zone. The shape of the branches $F_{\mathcal{A}}$ and $F_{\mathcal{C}}$ is similar to a quadratic polynomial, while shape of the branches $F_{\mathcal{B}}$ and $F_{\mathcal{D}}$ is similar to a cubic one.

In order to reproduce the bifurcation structure observable in map (1), the archetypal model has to replicate not only the shape of the function F but also how this shape depends on parameters. In map (1), the considered bifurcation structure appears under variation of parameters E_0 and χ_0. Numerical experiments show that that

- the parameter χ_0 influences mainly the branches $F_{\mathcal{A}}$ and $F_{\mathcal{C}}$. For increasing values of this parameter, the vertical offset of these branches increases but the overall shape of the branches remain approximately unchanged;
- the parameter E_0 influences mainly the branches $F_{\mathcal{B}}$ and $F_{\mathcal{D}}$. The kind of influence is different than in the previous case: for increasing E_0, the values $F_{\mathcal{B}}(d_1)$ and $F_{\mathcal{D}}(d_3)$ increase, while the values $F_{\mathcal{B}}(d_2)$ and $F_{\mathcal{D}}(d_0)$ remain approximately unchanged;

- additionally, both parameters E_0 and χ_0 influence the location of the discontinuity points of F.

.....

It follows from the definition of the function $f(x)$ (specifically, from Eq. (3c)) that if a point x belongs to an m-cycle of map (3), then the point $x + \frac{1}{2}$ belongs to a cycle as well. Therefore, only the following two cases are possible:

(A) The points x and $x + \frac{1}{2}$ belong to the same cycle. Then, this cycle has necessarily an even period with the same number and the same location of the points in the intervals $I_{\mathcal{A}} \cup I_{\mathcal{B}}$ and $I_{\mathcal{C}} \cup I_{\mathcal{D}}$. In the following, such cycles are referred to as symmetric cycles or cycles of type A.

(B) The points x and $x + \frac{1}{2}$ belong to different cycles. Then, the map has necessarily at least two coexisting cycles of the same period, referred to in the following as asymmetric cycles or cycles of type B.

3.3 Construction of the archetypal model

Let us now define a map with the properties similar to the ones described above. First, we scale the phase space of the model to the interval $[0, 1)$, i.e,

$$x_{n+1} = f(x_n) \bmod 1. \tag{3a}$$

Then, we fix the location of the discontinuity points to be

$$d_0 = 0, \quad d_1 = \tfrac{1}{4}, \quad d_2 = \tfrac{1}{2}, \quad d_3 = \tfrac{3}{4}, \tag{3b}$$

Indeed, numerical experiments evidence that the dependency of the discontinuity points on system parameters is not significant for the resulting bifurcation structure. To achieve the symmetry similar to the one defined by Eq. (2), we require

$$f(x) = \begin{cases} g(x) & \text{if } x \in I_{\mathcal{L}} = [d_0, d_2)\,, \\ g(x - d_2) + d_2 & \text{if } x \in I_{\mathcal{R}} = [d_2, 1)\,. \end{cases} \tag{3c}$$

On the partition $I_{\mathcal{L}}$, the function g is defined by two nonlinear branches:

$$g(x) = \begin{cases} g_{\mathcal{L}}(x) & \text{if } x \in I_{\mathcal{A}} = [d_0, d_1)\,, \\ g_{\mathcal{R}}(x) & \text{if } x \in I_{\mathcal{B}} = [d_1, d_2)\,. \end{cases} \tag{3d}$$

In this way, the function f is defined by four branches $f_{\mathcal{A}}$, $f_{\mathcal{B}}$, $f_{\mathcal{C}}$, and $f_{\mathcal{D}}$ corresponding to the branches $F_{\mathcal{A}}$, $F_{\mathcal{B}}$, $F_{\mathcal{C}}$, and $F_{\mathcal{D}}$ of the original map (1):

$$f(x) = \begin{cases} f_{\mathcal{A}}(x) = g_{\mathcal{L}}(x) & \text{if } x \in I_{\mathcal{A}} = [d_0, d_1)\,, \\ f_{\mathcal{B}}(x) = g_{\mathcal{R}}(x) & \text{if } x \in I_{\mathcal{B}} = [d_1, d_2)\,, \\ f_{\mathcal{C}}(x) = g_{\mathcal{L}}(x - d_2) + d_2 & \text{if } x \in I_{\mathcal{C}} = [d_2, d_3)\,, \\ f_{\mathcal{D}}(x) = g_{\mathcal{R}}(x - d_2) + d_2 & \text{if } x \in I_{\mathcal{D}} = [d_3, 1)\,. \end{cases} \tag{3e}$$

A suitable definition of the functions $g_{\mathcal{L}}$, $g_{\mathcal{R}}$ is a key issue in the development of the archetypal model. Here, an obvious choice is to define them by polynomial functions. As for the function $g_{\mathcal{L}}$, it turns out that its non-monotonicity is essential for the appearance of the considered bifurcation structure, so we define it by a quadratic polynomial:

$$g_{\mathcal{L}}(x) = a_{\mathcal{L}} x^2 + b_{\mathcal{L}} x + c_{\mathcal{L}} \tag{3f}$$

Here, a vertical displacement of the branches $f_{\mathcal{A}}$, $f_{\mathcal{C}}$ mimicking the shift of the branches $f_{\mathcal{A}}$, $f_{\mathcal{C}}$ in the original map (1) under variation of the parameter χ_0 is achieved by variation of the offset $c_{\mathcal{L}}$.
As for the definition of the function $g_{\mathcal{R}}$, numerical experiments show that it is not necessary to define it by a cubic polynomial. It turns out that the essential features of the bifurcation structure exhibited by the original map can be reproduced by using a linear function instead. The property of map (1) we have to maintain here is that the variation of parameters influences the value of the function at the left boundary of its domain and does not change the value on the right one. Accordingly, for the values d_1, d_2 given by Eq. (3b), we define the function $g_{\mathcal{R}}$ as follows

$$g_{\mathcal{R}}(x) = b_{\mathcal{R}} x + c_{\mathcal{R}} \qquad \text{with } b_{\mathcal{R}} = 4(g_{\mathcal{R}}(d_2) - g_{\mathcal{R}}(d_1)),\ c_{\mathcal{R}} = 2g_{\mathcal{R}}(d_1) - g_{\mathcal{R}}(d_2) \tag{3g}$$

Thus, the influence of the parameter E_0 on the branches $F_{\mathcal{B}}$ and $F_{\mathcal{D}}$ in the original map is mimicked by fixing the value $g_{\mathcal{R}}(d_2)$ while the value $g_{\mathcal{R}}(d_1)$ is varied, so that both the slope $b_{\mathcal{R}}$ and the offset $c_{\mathcal{R}}$ are changed simultaneously.
In order to maintain the shape of the function f similar to the one of the function F in the relevant parameter region, the parameters $a_{\mathcal{L}}$, $b_{\mathcal{L}}$, $c_{\mathcal{L}}$, $b_{\mathcal{R}}$, and $c_{\mathcal{R}}$ have to fulfill some fulfill some conditions. To this end we require the function $g_{\mathcal{L}}$ to be located above the diagonal (i.e., $g_{\mathcal{L}}(x) > x$ for all $x \in [0, \frac{1}{4}]$), to have a minimum in its application domain (i.e., $a_{\mathcal{L}} > 0$ and $x = -\frac{b_{\mathcal{L}}}{2a_{\mathcal{L}}} \in (0, \frac{1}{4})$), and to map the orbits into the domain of the function $g_{\mathcal{R}}$ (i.e., $g_{\mathcal{L}}(0) < \frac{1}{2}$, $g_{\mathcal{L}}(\frac{1}{4}) < \frac{1}{2}$). As for the function $g_{\mathcal{R}}$, it has to be contracting and increasing (i.e., $0 < b_{\mathcal{R}} < 1$), and to have no fixed points (i.e., $g_{\mathcal{R}}(\frac{1}{2}) > \frac{1}{2}$). Under these conditions, the shapes of the functions f are sufficiently close to each other and we can expect the map (3) to exhibit dynamics similar to map (1).
Varied parameters: $\alpha = -g_{\mathcal{R}}(\frac{1}{2})$, $\beta = c_{\mathcal{R}}$

Figure 1: Overall bifurcation structure in map (3). In (a), periods of cycles in the corresponding regions are indicated, some chains of regions associated with cycles of the same period are shown in different colors. In (b), the symbolic descriptions of the regions are specified, the chain of regions associated with 16-cycles is highlighted. Rectangels marked in (a) with A, B are shown in Figs. 2, 3, and 4(a),(b), respectively.

Figure 2: Regions associated (a) with the symmetric 16-cycle $\mathcal{O}_{\mathcal{A}^4\mathcal{B}^4\mathcal{C}^4\mathcal{D}^4}$ and (b) with the pair of asymmetric 16-cycle $\mathcal{O}_{\mathcal{A}^5\mathcal{B}^3\mathcal{C}^4\mathcal{D}^4}$ $\mathcal{O}_{\mathcal{A}^4\mathcal{B}^4\mathcal{C}^5\mathcal{D}^3}$. The chain or regions corresponding to period 16 is highlighted. Rectangle marked in (a) is shown magnified in (b).

4 Bifurcation structure in the archetypal model

An example of the 2D bifurcation structure in map (3) is shown in Fig. 1(a). As one can see, the structure is formed by partially overlapping regions associated with various cycles. It is worth noting that all cycles belonging to this structure have even periods. Recall that symmetric cycles of map (3) are necessarily of even periods, while the pairs of coexisting asymmetric cycles may have odd periods as well. However, such cycles do not appear within the considered bifurcation structure.

The cycles of period $2m$, $m \geqslant 2$, forming the considered bifurcation structure have points in all four partitions, and, more specifically, are associated with symbolic sequences $\mathcal{A}^{m_\mathcal{A}}\,\mathcal{B}^{m_\mathcal{B}}\,\mathcal{C}^{m_\mathcal{C}}\,\mathcal{D}^{m_\mathcal{D}}$ with $m_{\mathcal{A},\mathcal{B},\mathcal{C},D} > 0$, $m_\mathcal{A} + m_\mathcal{B} + m_\mathcal{C} + m_\mathcal{D} = 2m$. This follows from the restrictions for the parameter of function f mentioned in Sec. 3.3 which guarantee that from each partition the orbits are mapped into the next one. Moreover, the number of points in the corresponding partitions on the left and the right halves of the state space (i.e., in $I_\mathcal{A}$ and $I_\mathcal{C}$, as well as in $I_\mathcal{B}$ and $I_\mathcal{D}$) differs at most by one, i.e., $|m_\mathcal{A} - m_\mathcal{C}| \leqslant 1$, $|m_\mathcal{B} - m_\mathcal{D}| \leqslant 1$ (see Fig. 1(b))

As one can clearly see in Fig. 1(b), for each period $2m$, the bifurcation structure of map (3) contains a chain of pairwise overlapping periodicity regions of cycles with the same period $2m$ but differing in the corresponding symbolic sequences. Each chain start with the region associated with the symmetric cycle $\mathcal{O}_{\mathcal{A}^{m-1}\,\mathcal{B}\,\mathcal{C}^{m-1}\,\mathcal{D}}$ such that among m of its points located in each of the partitions $I_\mathcal{L}$ and $I_\mathcal{R}$, all but one are located in $I_\mathcal{A}$ and $I_\mathcal{C}$, respectively. Then, the chain is built up by consecutive movement of these points, one by one, from these intervals to the adjacent intervals $I_\mathcal{B}$ and $I_\mathcal{D}$. Graphically, the beginning of each chain can be illustrated by the following scheme:

$$\boxed{\mathcal{A}^{m-1}\,\mathcal{B}\,\mathcal{C}^{m-1}\,\mathcal{D}}\ \boxed{\begin{matrix}\mathcal{A}^{m-2}\,\mathcal{B}^2\,\mathcal{C}^{m-1}\,\mathcal{D}\\ \mathcal{A}^{m-1}\,\mathcal{B}\,\mathcal{C}^{m-2}\,\mathcal{D}^2\end{matrix}}\ \boxed{\mathcal{A}^{m-2}\,\mathcal{B}^2\,\mathcal{C}^{m-2}\,\mathcal{D}^2}\ \boxed{\begin{matrix}\mathcal{A}^{m-3}\,\mathcal{B}^3\,\mathcal{C}^{m-2}\,\mathcal{D}^2\\ \mathcal{A}^{m-2}\,\mathcal{B}^2\,\mathcal{C}^{m-3}\,\mathcal{D}^3\end{matrix}}\ \cdots \tag{4}$$

and a generic step in this scheme can be specified as follows

$$\cdots\ \boxed{\mathcal{A}^{m-k}\,\mathcal{B}^k\,\mathcal{C}^{m-k}\,\mathcal{D}^k}\ \boxed{\begin{matrix}\mathcal{A}^{m-(k+1)}\,\mathcal{B}^{k+1}\,\mathcal{C}^{m-k}\,\mathcal{D}^k\\ \mathcal{A}^{m-k}\,\mathcal{B}^k\,\mathcal{C}^{m-(k+1)}\,\mathcal{D}^{k+1}\end{matrix}}\ \cdots \tag{5}$$

with $0 < k < m$ (provided, the chain is not truncated).

As an example, Fig. 2 shows some of the regions forming the chain corresponding to period 16, specifically, the regions associated with a symmetric 16-cycle $\mathcal{O}_{\mathcal{A}^4\mathcal{B}^4\mathcal{C}^4\mathcal{D}^4}$ (see Fig. 2(a)) and with a pair of asymmetric 16-cycle $\mathcal{O}_{\mathcal{A}^5\mathcal{B}^3\mathcal{C}^4\mathcal{D}^4}$ $\mathcal{O}_{\mathcal{A}^4\mathcal{B}^4\mathcal{C}^5\mathcal{D}^3}$ (Fig. 2(b)). It is clearly visible that the regions overlap pairwise and that the number of points located in the partitions $I_\mathcal{A}$, $I_\mathcal{B}$ decreases along a chain, while the number of points in the partitions $I_\mathcal{B}$, $I_\mathcal{D}$ increases.

Each region in a chain has four boundaries corresponding to four border collision bifurcation curves. It is worth noting that due to the symmetry of the map, each border collision bifurcation in map (3) is a double border collision: either a border is collided by two points of the same symmetric cycle, or it is collided by two points of two coexisting asymmetric cycles.

Taking into account, that the points of a symmetric $2m$-cycle $\mathcal{O}_{\mathcal{A}^{m-k}\mathcal{B}^k\mathcal{C}^{m-k}\mathcal{D}^k}$ are located with respect to the border points as follows

$$\Big|\underbrace{x_0 \ldots x_{m-k-1}}_{d_0 \quad I_\mathcal{A}}\Big|\underbrace{x_{m-k} \ldots x_{m-1}}_{d_1 \quad I_\mathcal{B}}\Big|\underbrace{x_m \ldots x_{2m-k-1}}_{d_2 \quad I_\mathcal{C}}\Big|\underbrace{x_{2m-k} \ldots x_{2m-1}}_{d_3 \quad I_\mathcal{D}}\Big|_{d_0} \tag{6}$$

Figure 3: Border collision bifurcations confining the regions (a) $\mathcal{P}_{\mathcal{A}^4\mathcal{B}^4\mathcal{C}^4\mathcal{D}^4}$ and (b) $\mathcal{P}_{\mathcal{A}^5\mathcal{B}^3\mathcal{C}^4\mathcal{D}^4} \equiv \mathcal{P}_{\mathcal{A}^4\mathcal{B}^4\mathcal{C}^5\mathcal{D}^3}$. The chain of regions corresponding to period 16 is highlighted. Rectangle marked in (a) is shown magnified in (b). Parameter paths marked with A and B in (b) correspond to bifurcation diagrams shown in Fig. 4(a),(b), respectively.

we conclude that the border collision bifurcations this cycle can undergo are given by

$$\xi_{d_0,d_2}^{\underline{\mathcal{A}}^{m-k}\mathcal{B}^k\underline{\mathcal{C}}^{m-k}\mathcal{D}^k} = \{(\alpha,\beta) \mid x_0^{\mathcal{A}^{m-k}\mathcal{B}^k\mathcal{C}^{m-k}\mathcal{D}^k} = d_0 \text{ and } x_m^{\mathcal{A}^{m-k}\mathcal{B}^k\mathcal{C}^{m-k}\mathcal{D}^k} = d_2\} \tag{7}$$

$$\xi_{d_1,d_3}^{\underline{\mathcal{A}}^{m-k}\mathcal{B}^k\underline{\mathcal{C}}^{m-k}\mathcal{D}^k} = \{(\alpha,\beta) \mid x_{m-k-1}^{\mathcal{A}^{m-k-1}\mathcal{B}^k\mathcal{C}^{m-k}\mathcal{D}^k} = d_1 \text{ and } x_{2m-k-1}^{\mathcal{A}^{m-k}\mathcal{B}^k\mathcal{C}^{m-k}\mathcal{D}^k} = d_3\} \tag{8}$$

$$\xi_{d_1,d_3}^{\mathcal{A}^{m-k}\underline{\mathcal{B}}^k\mathcal{C}^{m-k}\underline{\mathcal{D}}^k} = \{(\alpha,\beta) \mid x_{m-k}^{\mathcal{A}^{m-k}\mathcal{B}^k\mathcal{C}^{m-k}\mathcal{D}^k} = d_1 \text{ and } x_{2m-k}^{\mathcal{A}^{m-k}\mathcal{B}^k\mathcal{C}^{m-k}\mathcal{D}^k} = d_3\} \tag{9}$$

$$\xi_{d_2,d_0}^{\mathcal{A}^{m-k}\underline{\mathcal{B}}^k\mathcal{C}^{m-k}\underline{\mathcal{D}}^k} = \{(\alpha,\beta) \mid x_{m-1}^{\mathcal{A}^{m-k}\mathcal{B}^k\mathcal{C}^{m-k}\mathcal{D}^k} = d_2 \text{ and } x_{2m-1}^{\mathcal{A}^{m-k}\mathcal{B}^k\mathcal{C}^{m-k}\mathcal{D}^k} = d_0\} \tag{10}$$

Note that in the notation for the border collision bifurcations the lower index refers to the discontinuities the cycle collides with and the upper one to the cycle undergoing the bifurcation. The underliened letters indicate which points of the cycle are colliding with the discontinuities: for example, the underliened letter $\mathcal{A}$ implies by Eq. (6) that either the point $x_0^{\mathcal{A}^{m-k}\mathcal{B}^k\mathcal{C}^{m-k}\mathcal{D}^k}$ collides with the discontinuity d_0 or the point $x_{m-k-1}^{\mathcal{A}^{m-k}\mathcal{B}^k\mathcal{C}^{m-k}\mathcal{D}^k}$ with d_1.
For the 16-cycle $\mathcal{O}_{\mathcal{A}^5\mathcal{B}^3\mathcal{C}^5\mathcal{D}^3}$, the four border collision bifurcations given by Eq. (7) are shown in Fig. 3(a). Note that at the corner points of the region $\mathcal{P}_{\mathcal{A}^5\mathcal{B}^3\mathcal{C}^5\mathcal{D}^3}$ the cycle undergoes codimension-2 border collision bifurcations at which it collides with all four discontinuities simultaneously.

Similar results can be obtained for a pair of coexisting asymmetric $2m$-cycles $\mathcal{O}_{\mathcal{A}^{m-k-1}\mathcal{B}^{k+1}\mathcal{C}^{m-k}\mathcal{D}^k}$ and $\mathcal{O}_{\mathcal{A}^{m-k}\mathcal{B}^k\mathcal{C}^{m-k-1}\mathcal{D}^{k+1}}$. One can easily see that their points are located with respect to the border points as follows

$$\Big|\underbrace{x_0\ldots x_{m-k-2}}_{d_0\qquad I_{\mathcal{A}}}\Big|\underbrace{x_{m-k-1}\ldots x_{m-1}}_{d_1\qquad I_{\mathcal{B}}}\Big|\underbrace{x_m\ldots x_{2m-k-1}}_{d_2\qquad I_{\mathcal{C}}}\Big|\underbrace{x_{2m-k}\quad\ldots x_{2m-1}}_{d_3\qquad I_{\mathcal{D}}}\Big|_{d_0} \tag{11}$$

$$\Big|\underbrace{x_0\ldots x_{m-k-1}}_{d_0\qquad I_{\mathcal{A}}}\Big|\underbrace{x_{m-k}\quad\ldots x_{m-1}}_{d_1\qquad I_{\mathcal{B}}}\Big|\underbrace{x_m\ldots x_{2m-k-2}}_{d_2\qquad I_{\mathcal{C}}}\Big|\underbrace{x_{2m-k-1}\ldots x_{2m-1}}_{d_3\qquad I_{\mathcal{D}}}\Big|_{d_0} \tag{12}$$

Therefore, the border collision bifurcations confining the periodicity regions of these cycles are

$$\xi_{d_0}^{\underline{\mathcal{A}}^{m-k-1}\mathcal{B}^{k+1}\mathcal{C}^{m-k}\mathcal{D}^k} = \{(\alpha,\beta) \mid x_0^{\mathcal{A}^{m-k-1}\mathcal{B}^{k+1}\mathcal{C}^{m-k}\mathcal{D}^k} = d_0\} \tag{13}$$

$$\xi_{d_2}^{\mathcal{A}^{m-k-1}\underline{\mathcal{B}}^{k+1}\mathcal{C}^{m-k}\mathcal{D}^k} = \{(\alpha,\beta) \mid x_{m-1}^{\mathcal{A}^{m-k-1}\mathcal{B}^{k+1}\mathcal{C}^{m-k}\mathcal{D}^k} = d_2\} \tag{14}$$

$$\xi_{d_3}^{\mathcal{A}^{m-k-1}\mathcal{B}^{k+1}\underline{\mathcal{C}}^{m-k}\mathcal{D}^k} = \{(\alpha,\beta) \mid x_{2m-k-1}^{\mathcal{A}^{m-k-1}\mathcal{B}^{k+1}\mathcal{C}^{m-k}\mathcal{D}^k} = d_3\} \tag{15}$$

$$\xi_{d_3}^{\mathcal{A}^{m-k-1}\mathcal{B}^{k+1}\mathcal{C}^{m-k}\underline{\mathcal{D}}^k} = \{(\alpha,\beta) \mid x_{2m-k}^{\mathcal{A}^{m-k-1}\mathcal{B}^{k+1}\mathcal{C}^{m-k}\mathcal{D}^k} = d_3\} \tag{16}$$

$$\xi_{d_1}^{\underline{\mathcal{A}}^{m-k}\mathcal{B}^k\mathcal{C}^{m-k-1}\mathcal{D}^{k+1}} = \{(\alpha,\beta) \mid x_{m-k-1}^{\mathcal{A}^{m-k}\mathcal{B}^k\mathcal{C}^{m-k-1}\mathcal{D}^{k+1}} = d_1\} \tag{17}$$

$$\xi_{d_1}^{\mathcal{A}^{m-k}\underline{\mathcal{B}}^k\mathcal{C}^{m-k-1}\mathcal{D}^{k+1}} = \{(\alpha,\beta) \mid x_{m-k}^{\mathcal{A}^{m-k}\mathcal{B}^k\mathcal{C}^{m-k-1}\mathcal{D}^{k+1}} = d_1\} \tag{18}$$

$$\xi_{d_2}^{\mathcal{A}^{m-k}\mathcal{B}^k\underline{\mathcal{C}}^{m-k-1}\mathcal{D}^{k+1}} = \{(\alpha,\beta) \mid x_m^{\mathcal{A}^{m-k}\mathcal{B}^k\mathcal{C}^{m-k-1}\mathcal{D}^{k+1}} = d_2\} \tag{19}$$

$$\xi_{d_0}^{\mathcal{A}^{m-k}\mathcal{B}^k\mathcal{C}^{m-k-1}\underline{\mathcal{D}}^{k+1}} = \{(\alpha,\beta) \mid x_{2m-1}^{\mathcal{A}^{m-k}\mathcal{B}^k\mathcal{C}^{m-k-1}\mathcal{D}^{k+1}} = d_0\} \tag{20}$$

As already mentioned, the existence regions $\mathcal{P}_{\mathcal{A}^{m-k}\mathcal{B}^k\mathcal{C}^{m-k-1}\mathcal{D}^{k+1}}$ and $\mathcal{P}_{\mathcal{A}^{m-k-1}\mathcal{B}^{k+1}\mathcal{C}^{m-k}\mathcal{D}^k}$ are identical and their borders coincide as follows

$$\xi_{d_0}^{\mathcal{A}^{m-k-1}\mathcal{B}^{k+1}\mathcal{C}^{m-k}\underline{\mathcal{D}}^k} \equiv \xi_{d_2}^{\mathcal{A}^{m-k}\underline{\mathcal{B}}^k\mathcal{C}^{m-k-1}\mathcal{D}^{k+1}} \tag{21}$$

$$\xi_{d_0}^{\underline{\mathcal{A}}^{m-k-1}\mathcal{B}^{k+1}\mathcal{C}^{m-k}\mathcal{D}^k} \equiv \xi_{d_2}^{\mathcal{A}^{m-k}\mathcal{B}^k\underline{\mathcal{C}}^{m-k-1}\mathcal{D}^{k+1}} \tag{22}$$

$$\xi_{d_1}^{\underline{\mathcal{A}}^{m-k-1}\mathcal{B}^{k+1}\mathcal{C}^{m-k}\mathcal{D}^k} \equiv \xi_{d_3}^{\mathcal{A}^{m-k}\mathcal{B}^k\underline{\mathcal{C}}^{m-k-1}\mathcal{D}^{k+1}} \tag{23}$$

$$\xi_{d_1}^{\mathcal{A}^{m-k-1}\underline{\mathcal{B}}^{k+1}\mathcal{C}^{m-k}\mathcal{D}^k} \equiv \xi_{d_3}^{\mathcal{A}^{m-k}\mathcal{B}^k\mathcal{C}^{m-k-1}\underline{\mathcal{D}}^{k+1}} \tag{24}$$

Figure 4: Bifurcation diagrams along the parameter paths intersecting the boundaries of the region $\mathcal{P}_{\mathcal{A}^5\mathcal{B}^3\mathcal{C}^4\mathcal{D}^4} \equiv \mathcal{P}_{\mathcal{A}^4\mathcal{B}^4\mathcal{C}^5\mathcal{D}^3}$ as indicated in Fig. 3. Parameters: (a) $\alpha = -0.375$; (b) $\beta = 0.1675$.

Figure 5: Number of coexisting attracting cycles (indicated by encircled numbers) close to the boundaries of the regions (a) $\mathcal{P}_{\mathcal{A}^4\mathcal{B}^4\mathcal{C}^4\mathcal{D}^4}$ and (b) $\mathcal{P}_{\mathcal{A}^5\mathcal{B}^3\mathcal{C}^4\mathcal{D}^4} \equiv \mathcal{P}_{\mathcal{A}^4\mathcal{B}^4\mathcal{C}^5\mathcal{D}^3}$. The chain or regions corresponding to period 16 is highlighted. Rectangle marked in (a) is shown magnified in (b). Coexisting attractors at the parameter values marked with A,B,C and D are shown in Fig. 6(a),(b), respectively.

as illustrated in Fig. 3(b) for the region $\mathcal{P}_{\mathcal{A}^5\mathcal{B}^3\mathcal{C}^4\mathcal{D}^4} \equiv \mathcal{P}_{\mathcal{A}^4\mathcal{B}^4\mathcal{C}^5\mathcal{D}^3}$. Note that at the corner points of this region, two codimension-2 border collision bifurcations occur. At these points, similar to the previous example, all four border points are collided, but here two of them are collided by the points of the cycle $\mathcal{O}_{\mathcal{A}^5\mathcal{B}^3\mathcal{C}^4\mathcal{D}^4}$ and the other two by points of $\mathcal{O}_{\mathcal{A}^4\mathcal{B}^4\mathcal{C}^5\mathcal{D}^3}$.

Examples of bifurcation diagrams across the boundaries of the region $\mathcal{P}_{\mathcal{A}^5\mathcal{B}^3\mathcal{C}^4\mathcal{D}^4} \equiv \mathcal{P}_{\mathcal{A}^4\mathcal{B}^4\mathcal{C}^5\mathcal{D}^3}$ are shown in Fig. 4. As illustrated in Fig. 4(a), at the border collision bifurcation $\xi_{d_3}^{\mathcal{A}^5\mathcal{B}^3\underline{\mathcal{C}}^4\mathcal{D}^4} \equiv \xi_{d_1}^{\underline{\mathcal{A}}^4\mathcal{B}^4\mathcal{C}^5\mathcal{D}^3}$ the asymmetric 16-cycles $\mathcal{O}_{\mathcal{A}^4\mathcal{B}^4\mathcal{C}^5\mathcal{D}^3}$ and $\mathcal{O}_{\mathcal{A}^5\mathcal{B}^3\mathcal{C}^4\mathcal{D}^4}$ collide with the border points d_1 and d_3, respectively. Additionally, in the same bifurcation diagram one can see the border collision bifurcation $\xi_{d_1,d_3}^{\mathcal{A}^4\underline{\mathcal{B}}^3\mathcal{C}^4\underline{\mathcal{D}}^3}$ of the symmetric 16-cycle $\mathcal{O}_{\mathcal{A}^4\mathcal{B}^4\mathcal{C}^4\mathcal{D}^4}$ which collides with the same discontinuities d_1,d_3 from the opposite side. Similarly, Fig. 4(a) shows the border collision bifurcation $\xi_{d_0}^{\underline{\mathcal{A}}^4\mathcal{B}^4\mathcal{C}^5\mathcal{D}^3} \equiv \xi_{d_2}^{\mathcal{A}^5\mathcal{B}^3\underline{\mathcal{C}}^4\mathcal{D}^4}$ at which the same pair of asymmetric 16-cycles $\mathcal{O}_{\mathcal{A}^5\mathcal{B}^3\mathcal{C}^4\mathcal{D}^4}$ and $\mathcal{O}_{\mathcal{A}^4\mathcal{B}^4\mathcal{C}^5\mathcal{D}^3}$ collide with the border points d_0 and d_2, respectively. In addition, the border collision bifurcation $\xi_{d_0,d_2}^{\mathcal{A}^5\underline{\mathcal{B}}^4\mathcal{C}^5\underline{\mathcal{D}}^4}$ of the symmetric 18-cycle $\mathcal{O}_{\mathcal{A}^5\mathcal{B}^4\mathcal{C}^5\mathcal{D}^4}$ collides with the same discontinuities from the opposite side. It is worth mentioning that in the considered bifurcation structure the border collision bifurcation curves do not intersect. However, it is possible that under variation of some parameters, such an intersection may occur. It is known [**?**] that in discontinuous 1D maps with a single border point and increasing branches, a codimension-2 border collision bifurcation at which two distinct cycles collide with the discontinuity from opposite sides acts as an organizing center of a period adding structure issuing from this point. This lead us to the question whether a similar structure can be expected to appear in map (3). This question is discussed in detail in our forthcoming work.

It can clearly be seen in Fig. 1 that not only regions forming a chain of regions of the same period overlap, but also each two adjacent chains overlap as well. This can be illustrated by the following diagram showing the changes of regions associated with cycles of period $2m$, surrounded by the chains associated with cycles of periods $2(m-1)$, and $2(m+1)$:

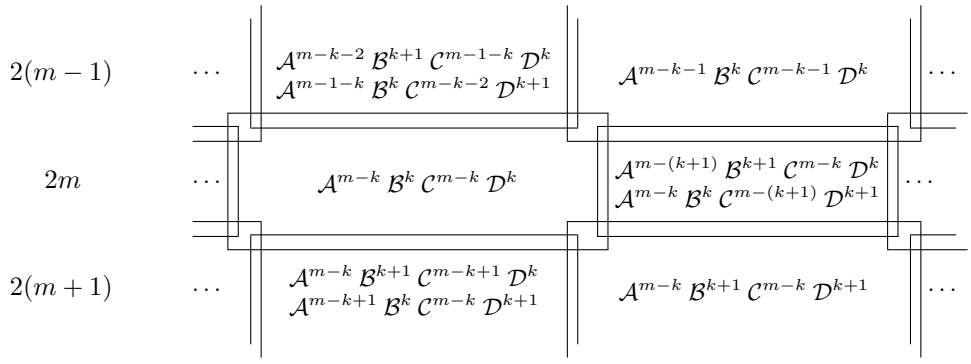

As one can see in this diagram, depending on actual parameter values, map (3) may exhibit either a single cycle or two, three, or four coexisting cycles. Indeed, each region associated with a pair of asymmetric $2m$-cycles has a non-empty overlap with a neighboring region associated with a symmetric cycle. Specifically, the region $\mathcal{P}_{\mathcal{A}^{m-(k+1)}\mathcal{B}^{k+1}\mathcal{C}^{m-k}\mathcal{D}^k} \equiv P_{\mathcal{A}^{m-k}\mathcal{B}^k\mathcal{C}^{m-(k+1)}\mathcal{D}^{k+1}}$ overlaps with

C1: the regions $\mathcal{P}_{\mathcal{A}^{m-k}\mathcal{B}^k\mathcal{C}^{m-k}\mathcal{D}^k}$ or $\mathcal{P}_{\mathcal{A}^{m-(k+1)}\mathcal{B}^{k+1}\mathcal{C}^{m-(k-1)}\mathcal{D}^{k+1}}$ belonging to the same chain. Accordingly, at the parameter values in these overlaps, map (3) exhibits three coexisting $2m$ cycles.

C2: the regions $\mathcal{P}_{\mathcal{A}^{m-k-1}\mathcal{B}^k\mathcal{C}^{m-k-1}\mathcal{D}^k}$ or $\mathcal{P}_{\mathcal{A}^{m-k}\mathcal{B}^{k+1}\mathcal{C}^{m-k}\mathcal{D}^{k+1}}$ belonging to the neighboring chains. In these overlaps, map (3) exhibits two coexisting $2m$-cycles and one $2(m-1)$- or $2(m+1)$-cycle.

Figure 6: Coexisting attracting cycles in map (3): (a) a symmetric 16-cycle $\mathcal{O}_{\mathcal{A}^5\mathcal{B}^3\mathcal{C}^5\mathcal{D}^3}$ and a symmetric 14-cycle $\mathcal{O}_{\mathcal{A}^4\mathcal{B}^3\mathcal{C}^4\mathcal{D}^3}$ at $\alpha = -0.4$, $\beta = 0.168$; (b) a pair of asymmetric 16-cycles $\mathcal{O}_{\mathcal{A}^5\mathcal{B}^3\mathcal{C}^4\mathcal{D}^4}$, $\mathcal{O}_{\mathcal{A}^4\mathcal{B}^4\mathcal{C}^5\mathcal{D}^3}$ at $\alpha = -0.375$, $\beta = 0.1678$; (c) a symmetric 14-cycle $\mathcal{O}_{\mathcal{A}^4\mathcal{B}^3\mathcal{C}^4\mathcal{D}^3}$ and a pair of asymmetric 16-cycles $\mathcal{O}_{\mathcal{A}^5\mathcal{B}^3\mathcal{C}^4\mathcal{D}^4}$, $\mathcal{O}_{\mathcal{A}^4\mathcal{B}^4\mathcal{C}^5\mathcal{D}^3}$ at $\alpha = -0.3797$, $\beta = 0.168$; (d) a symmetric 16-cycle $\mathcal{O}_{\mathcal{A}^5\mathcal{B}^3\mathcal{C}^5\mathcal{D}^3}$, a symmetric 14-cycle $\mathcal{O}_{\mathcal{A}^4\mathcal{B}^3\mathcal{C}^4\mathcal{D}^3}$, and a pair of asymmetric $\mathcal{O}_{\mathcal{A}^5\mathcal{B}^3\mathcal{C}^4\mathcal{D}^4}$, $\mathcal{O}_{\mathcal{A}^4\mathcal{B}^4\mathcal{C}^5\mathcal{D}^3}$ 16-cycles at $\alpha = -0.3805$, $\beta = 0.1672$. The basins of attraction are shown different colors. Corrsponding parameter values are indicated in Fig. 5.

Additionally, close it its corner points, the region $\mathcal{P}_{\mathcal{A}^{m-(k+1)}\mathcal{B}^{k+1}\mathcal{C}^{m-k}\mathcal{D}^k} \equiv P_{\mathcal{A}^{m-k}\mathcal{B}^k\mathcal{C}^{m-(k+1)}\mathcal{D}^{k+1}}$ overlaps with

C3: one of the regions $\mathcal{P}_{\mathcal{A}^{m-k}\mathcal{B}^k\mathcal{C}^{m-k}\mathcal{D}^k}$ or $\mathcal{P}_{\mathcal{A}^{m-(k+1)}\mathcal{B}^{k+1}\mathcal{C}^{m-(k-1)}\mathcal{D}^{k+1}}$ belonging to the same chain, and one of the regions $\mathcal{P}_{\mathcal{A}^{m-k-1}\mathcal{B}^k\mathcal{C}^{m-k-1}\mathcal{D}^k}$ or $\mathcal{P}_{\mathcal{A}^{m-k}\mathcal{B}^{k+1}\mathcal{C}^{m-k}\mathcal{D}^{k+1}}$ belonging to the neighboring chains. Hence, at the parameter values belonging to these overlaps, map (3) exhibits four coexisting cycles, namely three coexisting $2m$-cycles and one $2(m-1)$- or $2(m+1)$-cycle.

Moreover, as one can see in the above diagram, a region $\mathcal{P}_{\mathcal{A}^{m-k}\mathcal{B}^k\mathcal{C}^{m-k}\mathcal{D}^k}$ associated with a symmetric $2m$-cycle overlaps close to its corner point with

C4: another region associated with a symmetric cycle belonging to a neighboring chain, namely check it In these cases, map (3) exhibits coexistence of two symmetric cycles, one of period $2m$ and the other one of period $2(m+1)$ or $2(m-1)$.

It follows immediately that in all cases listed above the periods of coexisting cycles are either identical or differ by two.

To sum up, each region where map (3) has exactly two asymmetric cycles is surrounded by four regions where is has exactly three cycles (cases C1, C2), and by four regions where exactly four cycles coexist (case C3). Similarly, each region associated with a single (globally attracting) symmetric cycle is surrounded by four regions where the map has exactly two cycles (case C4), by four regions four regions where the map exhibits exactly three cycles (cases C1, C2), as well as eight regions where four cycles coexist (case C3). This is illustrated in Fig. 5, showing the number of attractors in the regions associated with a symmetric 16-cycle $\mathcal{O}_{\mathcal{A}^5\mathcal{B}^3\mathcal{C}^5\mathcal{D}^3}$ (Fig. 5(a)) and with a pair of asymmetric cycles $\mathcal{O}_{\mathcal{A}^5\mathcal{B}^3\mathcal{C}^4\mathcal{D}^4}$, $\mathcal{O}_{\mathcal{A}^4\mathcal{B}^4\mathcal{C}^5\mathcal{D}^3}$ (Fig. 5(b)). Examples of two, three and four coexisting cycles in the presented parameter region are shown in Fig. 6. Note that the basins of coexisting cycles are separated by the points of discontinuities and their preimages. Indeed, as at the considered parameter values the function f is everywhere contractive and therefore cannot have repelling cycles. Therefore, discontinuities and their preimages are the only points which can separate the basins, and the number of coexisting cycles cannot exceed twice the number of discontinuities (which corresponds to the case that each one-side-neighborhood of each discontinuity belongs to the basin of a different cycle). However, due to the symmetry 2 of the map, the neighborhoods of the discontinuities d_0, d_2, as well as of d_1, d_2 must belong to the same basins (e.g., if the left neighborhood of d_1 belongs to the basin of some cycle, then the left neighborhood of d_3 belongs to the basin of the same cycle). Accordingly, four is indeed the maximal number of coexisting cycles in the consideded map (see the example shown in Fig. 6(d)).

Figure 7: (b) $b_{\mathcal{L}} = 0.7$; (c) $b_{\mathcal{L}} = 0.9$; (d) $b_{\mathcal{L}} = 1.1$;

4.1 Changing the shape of f

Question: which properties are indeed important? We have already shown that the non-monotonicity of $F_{\mathcal{B}}$, $F_{\mathcal{D}}$ does not matter, thus the question arises whether the non-monotonicity of $F_{\mathcal{A}}$, $F_{\mathcal{C}}$ matters? Yes, it does, as illustrated in Fig. 7.